

1

2 **Separating isotopic impacts of karst and in-cave** 3 **processes from climate variability using an integrated** 4 **speleothem isotope-enabled forward model**

5 Pauline C. Treble^{1,3}, Mukhlis Mah^{2,3}, Alan Griffiths¹, Andy Baker^{2,3}, Michael
6 Deininger⁴, Bryce F. J. Kelly^{2,3}, Denis Scholz⁴, Stuart I. Hankin¹

7

8 ¹ANSTO, Lucas Heights, NSW 2234, Australia

9 ²Connected Waters Initiative Research Centre, UNSW Sydney, Sydney 2052, Australia

10 ³School of Biological, Earth and Environmental Sciences, UNSW Sydney, Sydney 2052, Australia

11 ⁴Institute for Geosciences, University of Mainz, Johann-Joachim-Becher-Weg 21, 55128 Mainz,
12 Germany

13 *Correspondence to:* Pauline Treble (pauline.treble@ansto.gov.au)

14

15 **Abstract.** Speleothem $\delta^{18}\text{O}$ values are commonly used to infer past climate variability. However, both
16 non-linear karst hydrological processes and in-cave disequilibrium isotope fractionation are recognised
17 and hinder the interpretation of $\delta^{18}\text{O}$ values. In recent years, proxy system models (PSMs) have
18 emerged to quantitatively assess the confounding effects of these processes. This study presents the
19 first integrated stalagmite $\delta^{18}\text{O}$ PSM (Karstolution) by coupling an existing karst hydrology with an in-
20 cave fractionation PSM. The new modelling framework not only couples the two models, but also
21 includes diffuse flow modelling, coupling of drip rate with infiltration, linking of surface with cave
22 temperature, and incorporates cave seasonality effects. We test Karstolution using a cave monitoring
23 dataset from Golgotha Cave, SW Australia. The predictive capacity of the model is assessed by
24 comparing the output to stalagmite $\delta^{18}\text{O}$ values. By comparing with observed stalagmite $\delta^{18}\text{O}$ values,
25 this study is also the first to quantify in-cave disequilibrium both kinetic isotopic fractionation in a
26 speleothem and informs the conclusion that hydroclimatic processes contributes more to the variability
27 of stalagmite $\delta^{18}\text{O}$ values at Golgotha Cave than does in-cave processes. This is further supported via a
28 sensitivity analysis performed by simulating the impacts of a wider range of cave temperature,
29 ventilation, drip interval and $p\text{CO}_2$ values than measured.

30

31 **Keywords:** proxy system model, speleothem, ISOLUTION, karst hydrology, oxygen isotopes

32

33

34 1 Introduction

35 Speleothems provide valuable paleoclimatic information due to their long time spans (10^2 - 10^4 years),
36 precise chronology, high resolution (sub-decadal to sub-annual depending on growth rate), and
37 relatively widespread distribution [McDermott, 2004]. The interpretation of speleothem $\delta^{18}\text{O}$ values is
38 still difficult due to the non-linearity of karst hydrology and in-cave isotopic fractionation (see
39 [Hartmann and Baker, 2017]).

40 Despite the common assumption that rainfall and cave dripwater $\delta^{18}\text{O}$ values have a linear relationship,
41 cave monitoring has revealed potential non-linear processes associated with variable infiltration of
42 recharge, mixing of various water stores, and non-linear water movement (e.g. [Ayalon et al., 1998;
43 Baker and Brunson, 2003; Fairchild et al., 2006; Mischel et al., 2015]. This can be further influenced
44 by: accentuation of high magnitude precipitation [Pape et al., 2010], mixing of different types of flow
45 (e.g. fracture and diffuse flow), and soil and epikarst evaporation [Cuthbert et al., 2014a].

46 Deposition of speleothem calcite under conditions of isotopic equilibrium implies isotopic equilibrium
47 between CaCO_3 , HCO_3^- and H_2O , such that the precipitated calcite is in isotopic equilibrium with the
48 water [Hendy, 1971]. However, many in-cave processes may prevent equilibrium isotopic
49 fractionation: (i) low relative humidity and in-cave air movement allow evaporative fractionation of
50 dripwater $\delta^{18}\text{O}$ values [Deininger et al., 2012]; (ii) high supersaturation of the dripwater with respect to
51 calcite (related to both cave and soil $p\text{CO}_2$) results in rapid precipitation after degassing of CO_2 , which
52 may disturb the isotope equilibrium between CaCO_3 , HCO_3^- and H_2O [Deininger et al., 2012; Mickler
53 et al., 2006; Scholz et al., 2009]; (iii) the time between two subsequent drips may affect the degree of
54 isotope disequilibrium [Deininger et al., 2012; Frisia et al., 2011; Kaufmann, 2003; Mühlinghaus et
55 al., 2007; Mühlinghaus et al., 2009; Riechelmann et al., 2013].

56 To advance our capacity to interpret the climatic record in speleothems, study sites are carefully
57 chosen, and monitoring of cave conditions, dripwater, and hydrology are established (e.g. [Baker et al.,
58 2014; Baldini et al., 2012; Duan et al., 2016; Frisia et al., 2011; Markowska et al., 2015; Spötl et al.,
59 2005]). However, quantification of the aforementioned processes is difficult, with issues outlined with
60 respect to the ‘Hendy Test’ [Dorale and Liu, 2009] and linear regression climate calibrations [Baker
61 and Bradley, 2010]. Replication from multiple stalagmites [Stoll et al., 2015], clumped isotope
62 thermometry ($\Delta 47$; [Affek et al., 2008] and analysis of fluid inclusions [Kluge et al., 2008] have been
63 proposed to demonstrate oxygen isotope equilibrium between water and speleothem calcite, but these
64 may be difficult to apply in practice.

65 To provide insights on the primary drivers of speleothem $\delta^{18}\text{O}$ variability, Proxy System Models
66 (PSMs) have emerged, using climatic inputs and numerical representation of the processes for forward
67 modelling of the proxies [Evans et al., 2013]. These models allow quantification of sensitivity to
68 various processes affecting proxy interpretation [Wong and Breecker, 2015]. The quantitative approach
69 of PSMs also facilitates simulations of ‘what-if’ climate scenarios to be compared against proxy data
70 (e.g. [Baker et al., 2012]), as well as assisting with constraining climate models, especially in the
71 emergent field of paleoclimate data assimilation (e.g. [Dee et al., 2016].

72 Hence, a number of karst and speleothem PSMs have been developed (Table 1). However, the majority
73 of the stalagmite $\delta^{18}\text{O}$ PSMs focus either on karst processes or in-cave processes and adopt a simplified
74 representation of the other part of the system. Of these, KarstFor [Bradley et al., 2010] and
75 ISOLUTION [Deininger et al., 2012], represent the most advanced treatment of the processes affecting
76 $\delta^{18}\text{O}$ values in the karst and cave, respectively.

77 Using a lumped parameter approach to model the complexities of karst hydrogeology, KarstFor was
78 first presented in Bradley et al. (2010) and subsequently enhanced with multiple adaptations (e.g.
79 [Baker and Bradley, 2010; Baker et al., 2013; Treble et al., 2013]. The initial iterations of KarstFor
80 consisted of climatic inputs (Table 2) and a monthly time-step for reservoirs representing the soil,
81 epikarst and vadose zone. This accounted for evaporative oxygen isotope fractionation in the soil store
82 and represented water-balance, mixing, overflow and underflow movement. The approach was highly
83 parameterised, thus requiring constraints by site-specific knowledge, and assumed in-cave equilibrium
84 isotope fractionation (using the [Kim and O’Neil, 1997] fractionation factor between water and calcite).

85

86 **Table 1: Summary of existing stalagmite and karst based forward models (PSMs) excluding catchment scale**
 87 **karst models.**

Model name	Description	Published
In-Cave Processes (No Karst Processes)		
	Model of stalagmite growth and $\delta^{13}\text{C}$ values on the stalagmite surface solution.	[Romanov <i>et al.</i> , 2008a; b]
ISOLUTION	Model of in-cave evaporation and isotope fractionation processes affecting stalagmite growth, $\delta^{13}\text{C}$ and $\delta^{18}\text{O}$ values.	[Deininger <i>et al.</i> , 2012; Mühlinghaus <i>et al.</i> , 2009; Scholz <i>et al.</i> , 2009]
	Stalagmite growth model based on in-cave conditions (drip saturation, $p\text{CO}_2$ and cave temperature) and climatic inputs.	[Kaufmann, 2003; Mühlinghaus <i>et al.</i> , 2007; Baker <i>et al.</i> , 2014]
I-STAL	Model of dripwater Mg, Sr and Ba from drip rate and drip saturation with respect to calcite; also represents prior calcite precipitation and dripwater chemistry.	[Stoll <i>et al.</i> , 2012]
	Model of the temporal isotopic ($\delta^{18}\text{O}$ and $\delta^{13}\text{C}$) evolution of DIC in a thin film precipitating calcite.	[Dreybrodt and Romanov, 2016]
Soil and In-Cave Processes (No Karst Processes)		
ODSM	Model of stalagmite $\delta^{18}\text{O}$ values from climatic input, soil mixing and vegetation effects. Soil water was modelled straight to in-cave and temperature dependent fractionation applied.	[Wackerbarth, 2012; Wackerbarth <i>et al.</i> , 2010; Wackerbarth <i>et al.</i> , 2012]
	Model of $\delta^{13}\text{C}$ and $\delta^{18}\text{O}$ values in soil (against soil $p\text{CO}_2$) and in-cave isotope fractionation processes.	[Dreybrodt and Scholz, 2011]
CaveCalc	PHREEQC-based model of soil, bedrock and in-cave processes including isotopes and trace elements	Owen <i>et al.</i> (2018)
Karst Processes (No In-Cave Processes)		
	Climatically fed single reservoir model with fracture flow for high magnitude rainfall and diffuse flow for low magnitude rainfall.	[Baker <i>et al.</i> , 2010; Nagra <i>et al.</i> , 2016]
	Two layer reservoir dripwater $\delta^{18}\text{O}$ model based on climatic input, with stores modelled as steady state.	[Truebe <i>et al.</i> , 2010]
KarstFor	Three (or four) layer reservoir model with soil evaporation, monthly water balance, overflow and underflow based on climatic input. Dripwater $\delta^{18}\text{O}$ values include temperature dependant isotope fractionation.	[Baker and Bradley, 2010; Baker <i>et al.</i> , 2013; Baker <i>et al.</i> , 2010; Fairchild and Baker, 2012; Jex <i>et al.</i> , 2013; Treble <i>et al.</i> , 2013]
	Two reservoir dripwater $\delta^{18}\text{O}$ model based on climatic input and defined residence time.	[Moerman <i>et al.</i> , 2014]
	Two layer reservoir model with daily water balance, mixing of $\delta^{18}\text{O}$ values and epikarst evaporation to model dripwater $\delta^{18}\text{O}$ values.	[Cuthbert <i>et al.</i> , 2014]
	Two reservoir discharge model with daily water balance.	Campbell <i>et al.</i> , 2017
KARSTMOD	Variable reservoir model of discharge at karst springs based on climatic input.	[Jourde <i>et al.</i> , 2015]
PRYSM	Open source GCM enabled single reservoir model using a mean transit time, τ . PRYSM includes models for other climate sensors (e.g. ice cores) and incorporates the errors associated with age assignments.	[Dee <i>et al.</i> , 2015]

88 ISOLUTION [Deininger et al., 2012] simulates speleothem $\delta^{18}\text{O}$ values in dependence of cave
89 temperature, drip interval, cave air pCO_2 , dripwater pCO_2 (an equivalent for the dripwater Ca^{2+}
90 concentration), relative humidity and cave ventilation during speleothem growth. ISOLUTION is based
91 on previous models describing speleothem growth and stable isotope fractionation (see [Deininger et
92 al., 2012] and [Deininger and Scholz, 2019] for details). By including in-cave oxygen isotope
93 disequilibrium and evaporative fractionation effects [Deininger et al., 2012], ISOLUTION is currently
94 the most advanced model describing speleothem oxygen isotope fractionation effects.

95 Here we present the first stalagmite $\delta^{18}\text{O}$ PSM combining karst and in-cave processes (Karstolution).
96 This integrated surface-to-stalagmite $\delta^{18}\text{O}$ PSM is a coupling of the KarstFor and ISOLUTION models
97 and allows for the first time the quantification of the effects of both karst and in-cave processes.
98 Karstolution includes the addition of diffuse flow, growth rate, modelling of in-cave seasonality and the
99 coupling of drip infiltration and cave temperature. We present a case study of Golgotha Cave using
100 monitoring data first presented by Treble et al. (2013) as well as data from recently deposited calcite.
101 Based on these data, we show how the Karstolution parameters can be localised to a particular cave site
102 and demonstrate how the model can be used to evaluate the relative effects of climatic, karst and in-
103 cave processes. As the conceptual model of Karstolution is generic it is not limited to Golgotha Cave
104 and can be applied to any karst setting.

105 2 Karstolution overview

106 Karstolution is a generic model that may be applied to many different karst settings, it couples KarstFor
107 and ISOLUTION and is the first integrated surface to stalagmite $\delta^{18}\text{O}$ PSM. The model is coded in
108 Python, with all code available on GitHub (<https://github.com/swasc/karstolution>). Karstolution is
109 based on a phenomenological representation of a karst system (Fig 1; Table 2) that is not derived from
110 fundamental laws. This has the advantage of limiting the model complexity, thus making it relatively
111 simple to reason with, fast to execute, and easier to configure. Disadvantages include: model
112 parameters that are not simple to relate to physical properties of the system, and limited ability to
113 precisely reproduce the observed time series. The model is mainly suited to hypothesis testing. For
114 example, isolating the impact of individual forcings, or varying these forcings through time. Model
115 calibration can be treated as an iterative process, beginning with a single active flow path, followed by
116 step-by-step introduction of more complexity.

117 The karst component of the model follows the KarstFor version presented in Baker et al. [2013], with
118 water levels in reservoirs (Soil Store, Epikarst, KS1 and KS2) given an initial value (mm) and then
119 recalculated (starting from the top store) at a monthly time step, via:

$$\Delta V = (\sum In - \sum Out) \Delta t$$

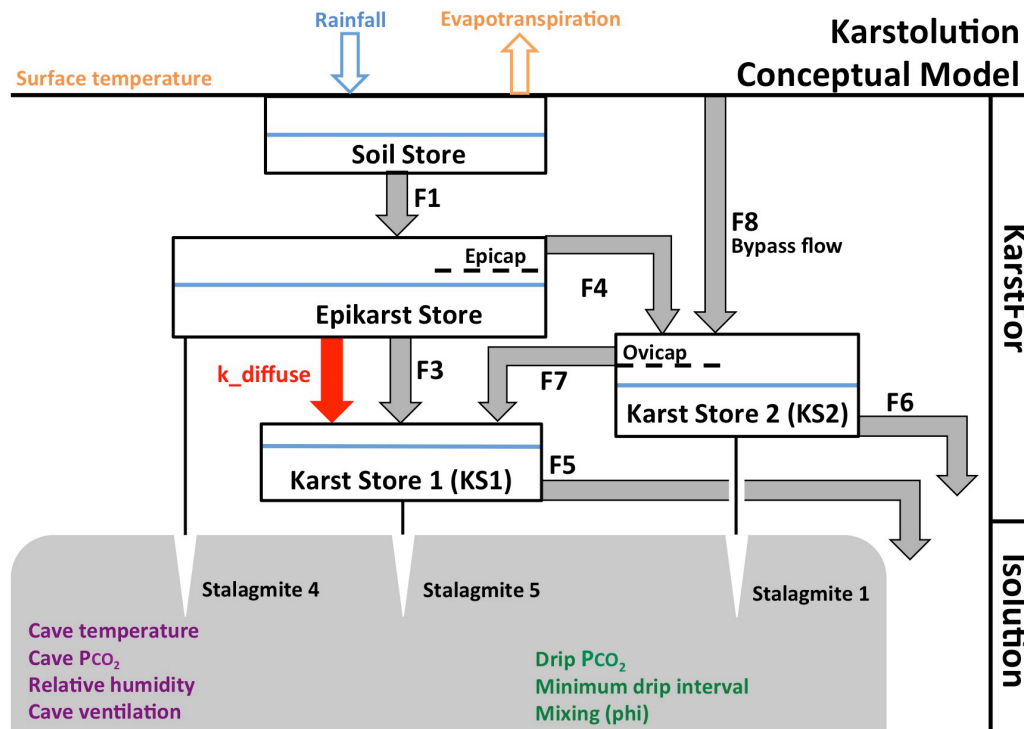
120 where ΔV = net change in store volume (mm) per month, In = input flows and Out = output flows
121 (mm/month) [either: fracture flow, diffuse flow or rainfall (Fig. 1)], and $\Delta t = 1$ month.

122 The $\delta^{18}\text{O}$ values in each store are updated with the time step based on the water balance calculations.
123 Three stalagmite outputs, representing multiple karst configurations, are modelled as per Baker et al.
124 [2013]. At each stalagmite output, the ISOLUTION model is applied to account for potential in-cave
125 fractionation processes, using the $\delta^{18}\text{O}$ value of the input reservoir water and the cave parameters
126 outlined in Table 2, to simulate stalagmite $\delta^{18}\text{O}$ values. For further description of the ISOLUTION
127 model, we refer the reader to Deininger et al. [2012] and Deininger and Scholz (2019). Additional
128 modelling capabilities: 1. in-cave seasonality, 2. diffuse flow, 3. the coupling of drip rate between the
129 KarstFor and ISOLUTION models, as well as 4. stalagmite growth rate) have been added and are
130 described below.

131 2.1 In-cave seasonality

132 The factors that may affect in-cave fractionation of $\delta^{18}\text{O}$ values can vary seasonally or at even higher
133 frequency [Baker et al., 2014; Markowska et al., 2015; Spötl et al., 2005; Treble et al., 2015]. For
134 example, seasonal cave ventilation can control cave air pCO_2 , an important factor affecting dripwater
135 supersaturation and, as a consequence, disequilibrium oxygen isotope fractionation, as well as leading
136 to seasonal biases in speleothem growth and geochemistry [Baldini et al., 2008; James et al., 2015;
137 Spötl et al., 2005]. As continuous cave parameter time series are rarely measured, it is not practical to

138 require this as an input series. Therefore, Karstolution allows the user to define seasonality of all
 139 factors that potentially affect in-cave oxygen isotope fractionation at their site through monthly
 140 averages of the cave parameters for each month of the year. The model additions in the next sections
 141 preserve this user-defined seasonality in its calculations.



142
 143 Figure 1. Conceptual figure of the Karstolution model. The boxes represent reservoirs, blue lines
 144 represent water levels, grey arrows represent fracture flow, and the red arrow represents diffuse flow.
 145 While a brief overview of the overall model is given in the main text, the details of the KarstFor and
 146 ISOLUTION models are given in Baker et al. [2013] and Deininger et al. [2012], respectively. Details
 147 of the coupling of the two models, modifications and additions are outlined in the main text. Each
 148 stalagmite output takes into account the effect of various cave parameters as described by ISOLUTION.
 149 See Table 2 for a summary of model inputs and parameters.

150 2.2 Dripwater coupling

151 The residence time of the surface water layer on the stalagmite controls the degree of the resulting
 152 isotopic disequilibrium [Deininger et al., 2012; Scholz et al., 2009]. As this residence time is dictated
 153 by the drip interval, which in turn is dependent on karst hydrology, modelling of the drip interval from
 154 the karst is necessary for application of ISOLUTION. We model drip-infiltration as gravity fed, with a
 155 linear response to the volume present in the karst store. Users specify the drip rate when the store is
 156 empty, q_0 , and full, q_1 , and the model calculates the instantaneous drip rate, q according to

$$q = (q_1 - q_0) \frac{ksize}{kstor} + q_0$$

157 where $ksize$ is the capacity of the karst store directly supplying the drip (mm) and $kstor$ is the current
 158 level of the karst store (mm; blue line in the stores shown in Fig. 1). The modelled drip interval, DI , is
 159 then

$$DI = \begin{cases} 1/q & q > 0 \\ 9001 & q \leq 0 \end{cases}$$

160 This allows for a choice of q_0 and q_1 where dripping stops before the store empties completely and
 161 represents the “no drip” state with a placeholder value.

162 **2.3 Temperature coupling**

163 Cave temperature is a key parameter for modelling stable isotope fractionation as well as the kinetics of
 164 calcite precipitation. Previously, the KarstFor model approximated cave air temperature as surface air
 165 temperature. However, this may not be the case due to the time taken for a surface heat signal to diffuse
 166 through bedrock [Dominguez-Villar et al., 2013]. Disequilibrium between surface and cave temperature
 167 may be affected by factors such as land use change, shading, fire, and rapid climate change
 168 [Dominguez-Villar et al., 2015; Nagra et al., 2016]. To deal with this, surface-cave temperature
 169 coupling is implemented in Karstolution with a site-specific difference between the ground surface and
 170 cave air temperature (ΔT_{s-c}). While maintaining ΔT_{s-c} , cave temperature varies using a user-defined
 171 moving average of the surface temperature (36-months in this study). A useful guide for temperature-
 172 depth penetration at different time periods is, for instance, presented in Fig. 9 of Rau et al. [2015].

173

174 **Table 2. Compilation of selected model parameter values with notes about their implementation and**
 175 **configuration. All parameter names are from conceptual Figure 1. Final configuration based on Treble et al.**
 176 **(2013) and updated here.**

Parameter	Description	Final configuration*
Soil store (mm)	Set to a small configuration with no soil evaporative fractionation as per field observations	Init: 150 Max: 500
Epikarst (mm)	Set to a small configuration with no epikarst evaporative fractionation as per field observations	Init: 30 Max: 50 Epicap: 35
KS1 (mm)	Primary karst store that receives flux from epikarst via k_diffuse and/or F3; may also receive overflow from KS2.	Init: 200 Max: 870
KS2 (mm)	Secondary karst store that fills via F4 and drains via F6 or permits modelling of switchable overflow to KS1 via F7. Magnitude of overflow is proportional to KS2/KS1 ratio.	Init: 1000 Max: 1400 Ovicap: 1150
F1 (mm/month)	Determines steady state values in soil store.	1.0
F3 (mm/month)	Flux representing fracture flow from Epikarst to KS1. Set to zero according to field observations of flow dominated by diffuse flow.	0
F4 (mm/month)	Flux from Epikarst to KS2 activated when threshold 'Epicap' is reached.	0.2
F5 (mm/month)	Drainage flux of KS1.	0.14
F7 (mm/month)	Overflow from KS2 back into KS1 once 'ovicap' is exceeded.	1.0
F6 (mm/month)	Drainage flux of KS2.	0.015
F8 (mm/month)	Bypass flow from the surface to KS2. Used to test configuration used by Treble et al. (2013) that KS2 was preferentially being recharged by rainfall events >7mm./month, but set to zero in final configuration.	0
k_diffuse (mm/month)	Flux is via pdf function to simulate diffuse flow.	0.5
ϕ	Mixing parameter of dripwater with the water layer on the stalagmite surface	1 (based on observations of limited drip splashing)
k_eevap	Fraction of water remaining in epikarst available to evaporate	0.1 (i.e. 10% per month)
k_d18O_soil	Isotopic evaporation coefficient for soil store	‰ month ⁻¹ mm ⁻¹
k_d18O_epi	Isotopic evaporation coefficient for epikarst store	‰ month ⁻¹ mm ⁻¹

177

178 **2.4 Diffuse flow**

179 Diffuse flow is an important addition to the previous fracture-flow-only versions of KarstFor [Baker
180 and Bradley, 2010], which would have poorly simulated sites with significant diffuse flow. Here,
181 diffuse flow includes flow through smaller fractures as well as the matrix and mathematically, no
182 mixing occurs along streamlines. Conversely, fracture flow is modelled as flow into reservoirs which
183 are immediately mixed. Following from the approach of Treble et al. (2013), Karstolution uses a
184 Weibull distribution to model diffuse flow. This was chosen because the Weibull distribution is a
185 generalisation of the Exponential and Rayleigh distributions, and has a variable shape and skewness
186 and hence can represent a large variety of possible transit time distributions [Almalki and Nadarajah,
187 2014]. The need to model variable flow distributions has been demonstrated for a novel D₂O irrigation
188 experiment at Wellington Caves (semi-arid, SE Australia), where cave dripwaters were shown to be a
189 mix of tracer, modern and paleo-water (see Fig. 4 of [Markowska et al., 2016]).

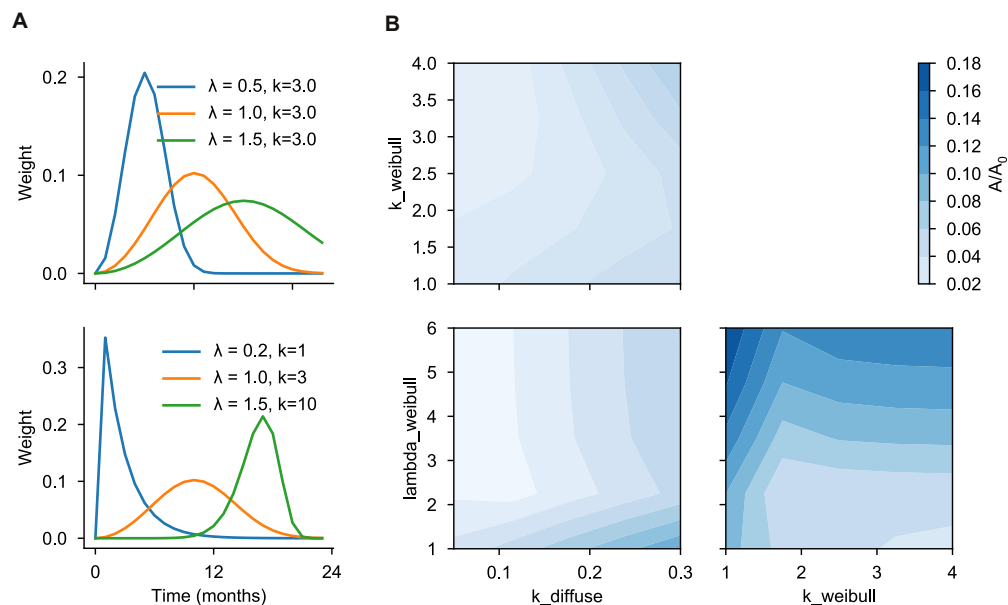
190 The two parameter Weibull distribution is represented as

$$f(x; \lambda, k) = \frac{k}{\lambda} \left(\frac{x}{\lambda}\right)^{k-1} e^{-\left(\frac{x}{\lambda}\right)^k}$$

where $x \geq 0, k > 0, \lambda > 0$.

191 The two parameters, k and λ , represent shape and scale, respectively (Fig. 2). The Weibull function is
192 implemented over the domain $0 \leq x \leq 2$, divided over an adjustable-length mixing window. At each
193 model step, k_{diffuse} determines the diffuse flow leaving the epikarst (see Table 2). This, along with
194 the values for the previous months, is multiplied by the corresponding weights (y-values from Fig. 2)
195 from the Weibull. The resulting flow entering KS1 (red arrow, Fig. 1) represents the diffuse flow
196 amount for that month. Here, this process is applied to both water fluxes and mixing of $\delta^{18}\text{O}$ values,
197 rather than just $\delta^{18}\text{O}$, as in Treble et al. (2013). It is implemented in the same manner every iteration
198 (i.e. there are no seasonal factors included in the diffuse flow).

199 As shown in Fig. 2, the Weibull parameters, k and λ , control the residence time distribution. The scale
200 parameter, k , controls where the peak occurs whereas the shape parameter, λ , can be used to change the
201 distribution from left-skewed to right-skewed. As well as introducing a lag into the system, the diffuse
202 flow parameterisation dampens the seasonal cycle. It does this more as the width of the peak increases,
203 as shown in Fig. 2.



204

205 **Figure 2. (a) Weibull distribution with parameters adjusted to change the peak width and shape. (b) the effect**
206 **of changing the diffuse flow parameterisation on the amplitude, A , of a sinusoidal $\delta^{18}\text{O}$ input series. The input**
207 **$\delta^{18}\text{O}$ series has a period of 12 months, amplitude of A_0 , monthly precipitation is held fixed, and other model**
208 **parameters are set to the configuration given in Table 2.**

209 2.5 Growth rate

210 The seasonal variation in speleothem growth rate can be important when comparing field observations
211 to model output because the mean observed $\delta^{18}\text{O}$ will be weighted towards periods of faster growth.
212 Speleothem growth rates are computed by Karstolution using the method presented by Kaufmann
213 (2008), based on Dreybrodt (1999), whereby the growth rate, W_0 , is

$$W_0 = 1.174 \times 10^3 (c - c_{\text{app}}) \frac{\delta}{\Delta d} \left[1 - \exp\left(-\frac{\alpha}{\delta} \Delta d\right) \right]$$

214 where c is the $p\text{CO}_2$ of water droplets, c_{app} is the apparent equilibrium $p\text{CO}_2$ of cave air ($1/\sqrt{0.8}$ times
215 the cave air $p\text{CO}_2$), δ is the water film thickness (set to 0.01 cm), Δd is the drop interval, α is a rate
216 constant, and the numerical factor is chosen so that W_0 has units of m year^{-1} . As with the calculation of
217 $\delta^{18}\text{O}$, there is an optional correction for drop splashing (detailed by *Deininger et al.*, 2012).

218 3 Site description

219 Golgotha Cave, SW Western Australia ($34^\circ 05' \text{S}$, $115^\circ 03' \text{E}$, Fig. 3), is located in a highly porous
220 Quaternary-age calcarenite of aeolian origin. The present-day climate is Mediterranean-type. The cave
221 is located at approximately 40 m depth under a wet eucalypt, evergreen forest (mixed *E. diversicolor*
222 and *E. calophylla*). Drip monitoring studies at Golgotha Cave have shown consistent drip-rates despite
223 the distinctly seasonal rainfall [*Treble et al.*, 2013]. LiDAR analysis coupled with high temporal and
224 spatial-resolution drip-logger studies confirmed the dominance of diffuse flow, temporally consistent
225 drip-rates and storage [*Mahmud et al.*, 2015; 2016; 2018]. For further details about Golgotha Cave
226 studies refer to *Treble et al.* [2013], *Treble et al.* [2016], *Mahmud et al.* [2015] and *Mahmud et al.*
227 [2016].



228

229 **Figure 3.** Location of Golgotha Cave in south-west Western Australia; the location of Calgardup Cave, where
230 rainfall samples were collected, is also shown. The reader is referred to Figure 3 in Mahmud et al. [2016] for
231 detailed site descriptions and maps.

232 4 Methods

233 4.1 Cave monitoring data

234 This study utilises data from August 2005 until March 2012 from Golgotha Cave that were previously
235 published in *Treble et al.* (2013). Procedures for rainwater and dripwater sampling and analytical
236 methods are presented in *Treble et al.* [2013; 2015].

237 The average cave parameters for each month of the year were determined by calculating the monthly
238 means of the following data originally acquired at 15 min intervals using a Datalogger DT80 logger
239 between May 2017 and April 2018:

- 240 • relative humidity with a Vaisala HMP155 with Humicap 180RC and sensor warming enabled
241 to negate saturation of the sensor at high humidity (accuracy $\pm 1.8\%$);
- 242 • cave temperature with a Vaisala independent temperature probe (accuracy $\pm 0.13^\circ\text{C}$);
- 243 • cave ventilation with a Gill Windsonic ($\pm 2\%$); and
- 244 • cave air $p\text{CO}_2$ with a Viasala GMP252 with measurement range 0-10,000 ppm (accuracy
245 ± 100 ppm). The longer cave air $p\text{CO}_2$ dataset (March 2009 – June 2014) presented in Treble
246 et al. (2015) was used to match the time period of drip $p\text{CO}_2$ data (Treble et al., 2015).

247

248 4.2 Modern stalagmite $\delta^{18}\text{O}$ values

249 To further validate the model, modern stalagmite $\delta^{18}\text{O}$ data from the drip sites were compared with the
250 model output. The method of sampling the modern calcite $\delta^{18}\text{O}$ is described in *Treble et al.* [2005].
251 Average stalagmite $\delta^{18}\text{O}$ values of approximately 10 years of growth preceding stalagmite sampling,
252 and the range of values at each site and analytical error (0.07‰, 2σ) was applied to quantify the
253 uncertainties.

254 5 Results

255 5.1.1 In-cave processes

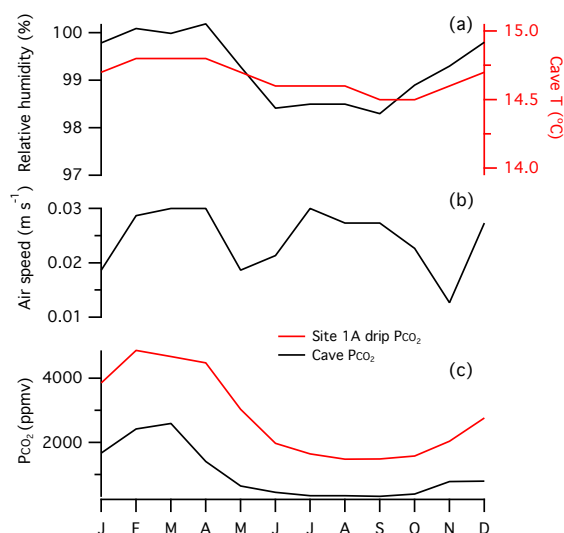
256 The monthly means from cave monitoring data used in the model are presented in Figs. 4a-c. Cave
257 temperature displays a smooth seasonal cycle, peaking in February-April but with low overall
258 variability (14.5-14.8°C; Fig. 4a). Other cave variables display similar seasonal maxima, also occurring
259 in late summer/early autumn. Relative humidity is high (98 -100%; Fig. 4a). Cave-air and dripwater
260 $p\text{CO}_2$ (Fig. 4b-c) demonstrate strong seasonality, reaching summer peaks of 2600 and 6800 ppmV and
261 winter minimums of 540 and 1000 ppmV, respectively. This and the subtler seasonal trend in relative
262 humidity are driven by temperature-driven gradients in seasonal cave ventilation (Treble et al., 2015)
263 although air speed measurements demonstrate that air movement in the cave is low ($\leq 0.03 \text{ m s}^{-1}$; Fig.
264 4b).

265

266 5.1.2 Stalagmite calcite $\delta^{18}\text{O}$ values

267 Stalagmite $\delta^{18}\text{O}$ values are compared to the simulated Karstolution output as well as the output
268 resulting from applying the equilibrium stable isotope fractionation factor of *Kim and O'Neil* [1997]
269 (Fig. 5). Since Karstolution accounts for in-cave evaporative and disequilibrium isotope fractionation
270 effects in addition to the equilibrium fractionation effect generated by the *Kim and O'Neil* [1997]
271 equation, comparing the two outputs enables us to quantify the impact of in-cave disequilibrium
272 fractionation. In general there is good agreement between the observed stalagmite $\delta^{18}\text{O}$ mean values
273 and modelled outputs for Site 1A (Fig. 5) indicating that this stalagmite is precipitating at near isotopic
274 equilibrium. The seasonal maxima of the Karstolution outputs overlap with the observed stalagmite
275 means. This is consistent with the expectation that stalagmite deposition in Golgotha Cave will be
276 biased towards the cooler months (Treble et al., 2015) and indicates that non-equilibrium processes
277 may be more enhanced when the cave is in ventilated mode.

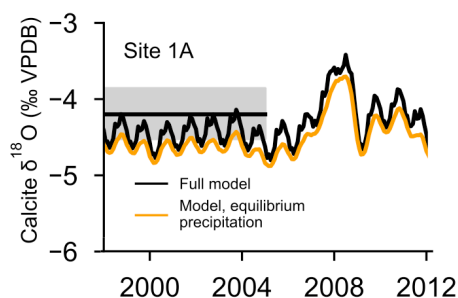
278



279

280 **Figure 4: (a) Average monthly values for relative humidity and cave temperature. (b) Average monthly values**
 281 **for air speed. (c) Cave pCO₂ and calculated dripwater pCO₂ values. Calculated dripwater pCO₂ values are the**
 282 **dripwater pCO₂ values restored to calcite saturation (see Treble et al., 2015).**

283



284

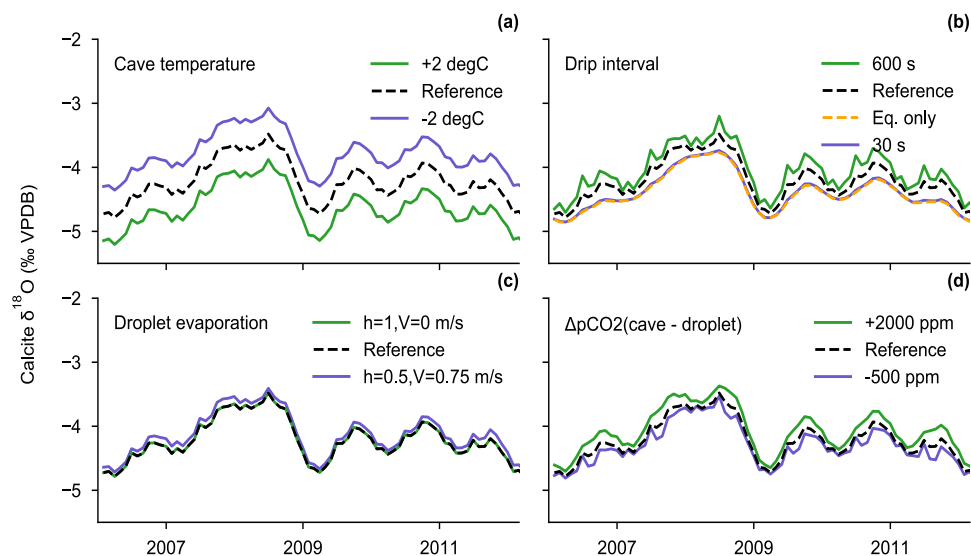
285 **Figure 5. Comparison of observed stalagmite δ¹⁸O values (grey bars) with modelled stalagmite δ¹⁸O (orange:**
 286 **modelled dripwater δ¹⁸O output converted to calcite assuming equilibrium oxygen isotope fractionation; black:**
 287 **full Karstolution output with ISOLUTION model enabled).**

288

289 A sensitivity analysis was performed to determine which cave parameters potentially drive stalagmite
 290 δ¹⁸O variability at Golgotha Cave. Figure 6 shows a reference case based on Site 1A, along with
 291 perturbations to cave parameters (Fig. 4). It demonstrated that the isotopic impact of temperature
 292 should be considered once mean cave temperature variability exceeds ±2°C (i.e., greater than that
 293 expected for the Holocene).

294 In terms of the potential isotopic impact of disequilibrium processes, stalagmite δ¹⁸O appears to have
 295 some sensitivity to drip interval over the observed range for Golgotha Cave (Fig. 6b). The degree of
 296 disequilibrium increases at longer drip intervals as indicated by the departure from the predicted
 297 equilibrium δ¹⁸O values. This is consistent with the expectation that deviation from isotopic
 298 equilibrium increases with the degree of calcite precipitation (Mühlinghaus et al., 2009; Deininger et al.,
 299 2012) before another drip falls. The sensitivity to changes in relative humidity and cave air movement
 300 are negligible due to the low variability of these parameters at Golgotha Cave (Fig. 6). The latter is in
 301 agreement with findings of negligible disequilibrium isotopic fractionation effects provided cave
 302 ventilation is less than 0.2 m/s and relative humidity greater than 85% [Deininger et al., 2012;
 303 Dreybrodt and Deininger, 2014], and indicates that in-cave evaporative fractionation is not a driver of
 304 stalagmite δ¹⁸O variability in this karst setting. Finally, the sensitivity of stalagmite δ¹⁸O at Site 1A to

305 the gradient between dripwater and cave $p\text{CO}_2$ is small to negligible (Fig. 6d), although this effect may
 306 become more important if the drip interval at this site were to increase (Fig. 6b).
 307



308

309 Figure 6. Sensitivity analysis for cave parameters at drip Site 1A: (a) cave temperature. (b) drip interval
 310 (c) relative humidity and cave ventilation. (d) cave air minus dripwater $p\text{CO}_2$. In order to preserve the
 311 measured seasonality in cave parameters, the reference case uses monthly values from Fig. 4 and
 312 perturbations have a constant offset across all months, with the addition of a limit to physically-realistic
 313 values (e.g. humidity must lie in the range 0-1). The predicted equilibrium calcite $\delta^{18}\text{O}$ from Figure 5 is
 314 also reproduced on Figure 6b for comparison.

315 6 Discussion

316

317 The cave-parameter sensitivity analysis (Fig. 6) demonstrated sensitivity of Golgotha Cave stalagmite
 318 $\delta^{18}\text{O}$ to cave temperature and drip interval and minimal isotopic effects of changes in evaporation and
 319 the cave air and dripwater $p\text{CO}_2$ gradient. Modelling the effects of in-cave disequilibrium isotope and
 320 evaporative fractionation over that of equilibrium isotope fractionation (Fig. 5) shows that at Golgotha
 321 Cave disequilibrium effects contribute negligibly to stalagmite $\delta^{18}\text{O}$ variability (Fig. 5). It is
 322 emphasised here that disequilibrium is accounted for in Karstolution, whereas kinetic fractionation is
 323 not. Disequilibrium isotope fractionation modelled by Karstolution accounts for the disturbance of the
 324 isotope equilibrium between CaCO_3 , HCO_3^- and H_2O . In contrast, kinetic isotope fractionation
 325 represents the change of the isotope fractionation factor in relation to e.g., the precipitation rate (see
 326 Dietzl et al. 2009). Thus kinetic fractionation could be viewed as the offset between the Karstolution
 327 modelled values and the observed speleothem $\delta^{18}\text{O}$, implying that kinetic fractionation effects also have
 328 small to negligible isotopic impact on Golgotha Cave stalagmites. Adopting other fractionation factors
 329 (e.g. Coplen, 2007) may result in larger offsets compared to the predicted equilibrium output and may
 330 be appropriate for other locations.

331 One of the major advantages of Karstolution compared to previous stalagmite $\delta^{18}\text{O}$ PSMs is the
 332 isolation of various factors affecting isotopic values. For example, in analysing a Scottish millennial-
 333 length stalagmite with KarstFor, Baker et al. [2012] noted there was uncertainty if in-cave fractionation
 334 effects occur. In addition, integration of temperature-dependence of precipitation kinetics during calcite
 335 deposition, allows better representation and analysis of the effects of temperature and climate
 336 variability on stalagmite $\delta^{18}\text{O}$ values. This enables novel studies about both karst and cave effects, such
 337 as simulations of glacial-interglacial transitions, investigation of evaporative cooling [Cuthbert et al.,
 338 2014b; Rau et al., 2015] and the simulation of fire impacts, which increase soil evaporation and
 339 decrease the calcium content of the dripwater [Nagra et al., 2016]. The ability to competently model

340 these processes is critical in stalagmite $\delta^{18}\text{O}$ PSMs, augmenting the ability of these records to provide
341 accurate quantifications of uncertainty in climate models.

342 7 Conclusions

343 This study represents the first integrated stalagmite $\delta^{18}\text{O}$ PSM: representing both karst hydrological and
344 in-cave isotope fractionation processes. The primary assumptions incorporated into Karstolution have
345 been conditionally confirmed based on its ability to generally simulate measured drip rate response and
346 measured stalagmite $\delta^{18}\text{O}$ values. At Golgotha Cave, it is concluded that stalagmite $\delta^{18}\text{O}$ variability in
347 the model is primarily driven by climatic inputs and the karst system rather than in-cave processes.

348 Future research will include model confirmation of Karstolution at other sites of different climates and
349 hydrogeologies world-wide. Further modelling of the impacts of fire are also warranted. Future
350 combination of Karstolution with GCMs and large climate models could also allow analysis of long-
351 term model performance and facilitate realistic estimates of the variability of $\delta^{18}\text{O}$ values from the
352 surface to the stalagmite.

353

354 Acknowledgments

355 We would like to thank Martin Andersen and Sylvia Dee for their comments on an earlier draft of the
356 manuscript. We gratefully acknowledge the contributions of Nerilie Abram and Michael Gagan for
357 laboratory analysis of speleothem $\delta^{18}\text{O}$ data and Petra Bajo and John Hellstrom for U-series chronology
358 data that were utilised to calculate mean speleothem $\delta^{18}\text{O}$ values reported here. We also thank Barbora
359 Gallagher for water isotope analyses, the Calgardup Caves staff (Department of Parks and Wildlife) for
360 assisting with the cave monitoring data utilised here and Stuart Hankin for technical assistance in
361 acquiring these data and drafting Fig. 3. This study contributes to ARC Discovery Project
362 DP140102059 awarded to PCT and to ARC Linkage Project LP130100177 awarded to AB and PCT.
363 MM was supported by DAAD funding. MD and DS acknowledges funding of the DFG through grants
364 DE 2398/3-1 and SCHO 1274/9-1, respectively..

365

366 **References**

- 367 Affek, H. P., M. Bar-Matthews, A. Ayalon, A. Matthews, and J. M. Eiler (2008), Glacial/interglacial
368 temperature variations in Soreq cave speleothems as recorded by 'clumped isotope' thermometry,
369 *Geochimica et Cosmochimica Acta*, 72(22), 5351-5360.
- 370 Ayalon, A., M. Bar-Matthews, and E. Sass (1998), Rainfall-recharge relationships within a karstic
371 terrain in the Eastern Mediterranean semi-arid region, Israel: $\delta^{18}\text{O}$ and δD characteristics, *Journal of*
372 *Hydrology*, 207(1), 18-31.
- 373 Baker, A., and C. Brunson (2003), Non-linearities in dripwater hydrology: an example from Stump
374 Cross Caverns, Yorkshire, *Journal of Hydrology*, 277(3-4), 151-163.
- 375 Baker, A., and C. Bradley (2010), Modern stalagmite $\delta^{18}\text{O}$: Instrumental calibration and forward
376 modelling, *Global and Planetary Change*, 71(3-4), 201-206.
- 377 Baker, A., C. Bradley, and S. J. Phipps (2013), Hydrological modeling of stalagmite $\delta^{18}\text{O}$ response to
378 glacial-interglacial transitions, *Geophysical Research Letters*, 40(12), 3207-3212.
- 379 Baker, A., C. Bradley, S. J. Phipps, M. Fischer, I. J. Fairchild, L. Fuller, C. Spötl, and C. Azcurra
380 (2012), Millennial-length forward models and pseudoproxies of stalagmite $\delta^{18}\text{O}$: an example from NW
381 Scotland, *Climate of the Past*, 8(4), 1153-1167.
- 382 Baker, A., A. Asrat, I. J. Fairchild, M. J. Leng, L. Thomas, M. Widmann, C. N. Jex, Buwen Dong, P.
383 van Calsteren, and C. Bryant (2010), Decadal-scale rainfall variability in Ethiopia recorded in an
384 annually laminated, Holocene-age, stalagmite, *The Holocene*, 20(6), 827-836.
- 385 Baker, A. J., D. P. Matthey, and J. U. L. Baldini (2014), Reconstructing modern stalagmite growth from
386 cave monitoring, local meteorology, and experimental measurements of dripwater films, *Earth and*
387 *Planetary Science Letters*, 392, 239-249.
- 388 Baldini, J. U. L., F. McDermott, L. M. Baldini, C. J. Ottley, K. L. Linge, N. Clipson, and K. E. Jarvis
389 (2012), Identifying short-term and seasonal trends in cave dripwater trace element concentrations based
390 on a daily-scale automatically collected dripwater dataset, *Chemical Geology*, 330-331, 1-16.
- 391 Bradley, C., A. Baker, C. N. Jex, and M. J. Leng (2010), Hydrological uncertainties in the modelling of
392 cave drip-water $\delta^{18}\text{O}$ and the implications for stalagmite palaeoclimate reconstructions, *Quaternary*
393 *Science Reviews*, 29(17-18), 2201-2214.
- 394 Coplen, T.B. (2007), Calibration of the calcite-water oxygen-isotope geothermometer at Devils Hole,
395 Nevada, a natural laboratory. *Geochimica et Cosmochimica Acta* 71, 3948-3957.
- 396 Cuthbert, M. O., A. Baker, C. N. Jex, P. W. Graham, P. C. Treble, M. S. Andersen, and I. R. Acworth
397 (2014a), Dripwater isotopes in semi-arid karst: Implications for speleothem paleoclimatology, *Earth*
398 *and Planetary Science Letters*, 395, 194-204.
- 399 Cuthbert, M. O., et al. (2014b), Evaporative cooling of speleothem dripwater, *Scientific reports*, 4,
400 5162.
- 401 Dee, S. G., N. J. Steiger, J. Emile-Geay, and G. J. Hakim (2016), On the utility of proxy system models
402 for estimating climate states over the common era, *Journal of Advances in Modeling Earth Systems*,
403 8(3), 1164-1179.
- 404 Deininger, M., & Scholz, D. (2019). ISOLUTION 1.0: an ISotope evoLUTION model describing the
405 stable oxygen ($\delta^{18}\text{O}$) and carbon ($\delta^{13}\text{C}$) isotope values of speleothems. *International Journal of*
406 *Speleology*, 48, 3. doi:<https://doi.org/10.5038/1827-806X.48.1.2219>
- 407 Deininger, M., J. Fohlmeister, D. Scholz, and A. Mangini (2012), Isotope disequilibrium effects: The
408 influence of evaporation and ventilation effects on the carbon and oxygen isotope composition of
409 speleothems – A model approach, *Geochimica et Cosmochimica Acta*, 96, 57-79.
- 410 Dietzel, M., J. Tang, A. Leis, and S. J. Köhler (2009), Oxygen isotopic fractionation during inorganic
411 calcite precipitation — Effects of temperature, precipitation rate and pH, *Chemical Geology*, 268, 107-
412 115.
- 413 Dorale, J. A., and Z. Liu (2009), Limitations of hendy test criteria in judging the paleoclimatic
414 suitability of speleothems and the need for replication, *Journal of Cave and Karst Studies*, 71(1), 73-80.

- 415 Dreybrodt, W., and M. Deininger (2014), The impact of evaporation to the isotope composition of DIC
416 in calcite precipitating water films in equilibrium and kinetic fractionation models, *Geochimica et*
417 *Cosmochimica Acta*, 125, 433-439.
- 418 Duan, W. H., J. Y. Ruan, W. J. Luo, T. Y. Li, L. J. Tian, G. N. Zeng, D. Z. Zhang, Y. J. Bai, J. L. Li, T.
419 Tao, P. Z. Zhang, A. Baker and M. Tan (2016), The transfer of seasonal isotopic variability between
420 precipitation and dripwater at eight caves in the monsoon regions of China, *Geochimica et*
421 *Cosmochimica Acta*, 183, 250-266.
- 422 Evans, M. N., S. E. Tolwinski-Ward, D. M. Thompson, and K. J. Anchukaitis (2013), Applications of
423 proxy system modeling in high resolution paleoclimatology, *Quaternary Science Reviews*, 76, 16-28.
- 424 Fairchild, I. J., G. W. Tuckwell, A. Baker, and A. F. Tooth (2006), Modelling of dripwater hydrology
425 and hydrogeochemistry in a weakly karstified aquifer (Bath, UK): Implications for climate change
426 studies, *Journal of Hydrology*, 321(1-4), 213-231.
- 427 Frisia, S., I. J. Fairchild, J. Fohlmeister, R. Miorandi, C. Spötl, and A. Borsato (2011), Carbon mass-
428 balance modelling and carbon isotope exchange processes in dynamic caves, *Geochimica et*
429 *Cosmochimica Acta*, 75(2), 380-400.
- 430 Hartmann, A. and A. Baker (2017), Modelling karst vadose zone hydrology and its relevance for
431 paleoclimate reconstruction, *Earth Science Reviews*, 172, 178-192.
- 432 Hendy, C. H. (1971), The isotopic geochemistry of speleothems—I. The calculation of the effects of
433 different modes of formation on the isotopic composition of speleothems and their applicability as
434 palaeoclimatic indicators, *Geochimica et Cosmochimica Acta*, 35(8), 801-824.
- 435 Jones, D. A., W. Wang, and R. Fawcett (2009), High-quality spatial climate data-sets for Australia."
436 *Australian Meteorological and Oceanographic Journal* 58(4), 233.
- 437 Kaufmann, G. (2003), Stalagmite growth and palaeo-climate: the numerical perspective, *Earth and*
438 *Planetary Science Letters*, 214(1-2), 251-266.
- 439 Kim, S.-T., and J. R. O'Neil (1997), Equilibrium and nonequilibrium oxygen isotope effects in
440 synthetic carbonates, *Geochimica et Cosmochimica Acta*, 61(16), 3461-3475.
- 441 Kluge, T., T. Marx, D. Scholz, S. Niggemann, A. Mangini, and W. Aeschbach-Hertig (2008), A new
442 tool for palaeoclimate reconstruction: Noble gas temperatures from fluid inclusions in speleothems,
443 *Earth and Planetary Science Letters*, 269(3-4), 408-415.
- 444 Mahmud, K., G. Mariethoz, P. C. Treble, and A. Baker (2015), Terrestrial LiDAR Survey and
445 Morphological Analysis to Identify Infiltration Properties in the Tamala Limestone, Western Australia,
446 *IEEE Journal of Selected Topics in Applied Earth Observations and Remote Sensing*, 8(10), 4871-4881.
447 doi: 10.1109/JSTARS.2015.2451088
- 448 Mahmud, K., G. Mariethoz, A. Baker, P. C. Treble, M. Markowska, and E. McGuire (2016),
449 Estimation of deep infiltration in unsaturated limestone environments using cave lidar and drip count
450 data, *Hydrol. Earth Syst. Sci.*, 20(1), 359-373. doi:10.5194/hess-20-359-2016
- 451 Mahmud, K., G. Mariethoz, A. Baker, and P.C. Treble, P.C. (2018), Hydrological characterization of
452 cave drip waters in a porous limestone: Golgotha Cave, Western Australia, *Hydrological and Earth*
453 *System Sciences* 22, 977-988. <https://doi.org/10.5194/hess-22-977-2018>
- 454 Markowska, M., A. Baker, P. C. Treble, M. S. Andersen, S. I. Hankin, C. N. Jex, C. V. Tadros, and R.
455 Roach (2015), Unsaturated zone hydrology and cave drip discharge water response: Implications for
456 speleothem paleoclimate record variability, *Journal of Hydrology*, 529, 662-675.
- 457 McDermott, F. (2004), Palaeo-climate reconstruction from stable isotope variations in speleothems: a
458 review, *Quaternary Science Reviews*, 23(7-8), 901-918.
- 459 Mickler, P. J., L. A. Stern, and J. L. Banner (2006), Large kinetic isotope effects in modern
460 speleothems, *Geological Society of America Bulletin*, 118(1-2), 65-81.
- 461 Mischel, S., D. Scholz, and C. Spötl (2015), $\delta^{18}\text{O}$ values of cave dripwater: a promising proxy for the
462 reconstruction of the North Atlantic Oscillation?, *Clim Dyn*, 1-16.

- 463 Mühlinghaus, C., Scholz, D. and Mangini, A. (2007), Modelling stalagmite growth and $\delta^{13}\text{C}$ as a
464 function of drip interval and temperature, *Geochimica et Cosmochimica Acta* 71, 2780-2790.
- 465 Mühlinghaus, C., D. Scholz, and A. Mangini (2009), Modelling fractionation of stable isotopes in
466 stalagmites, *Geochimica et Cosmochimica Acta*, 73(24), 7275-7289.
- 467 Nagra, G., P. C. Treble, M. S. Andersen, I. J. Fairchild, K. Coleborn, and A. Baker (2016), A post-
468 wildfire response in cave dripwater chemistry, *Hydrology and Earth System Sciences*, 20(7), 2745-
469 2758.
- 470 Pape, J. R., J. L. Banner, L. E. Mack, M. Musgrove, and A. Guilfoyle (2010), Controls on oxygen
471 isotope variability in precipitation and cave dripwaters, central Texas, USA, *Journal of Hydrology*,
472 385(1-4), 203-215.
- 473 Rau, G. C., M. O. Cuthbert, M. S. Andersen, A. Baker, H. Rutledge, M. Markowska, H. Roshan, C. E.
474 Marjo, P. W. Graham, and R. I. Acworth (2015), Controls on cave dripwater temperature and
475 implications for speleothem-based paleoclimate reconstructions, *Quaternary Science Reviews*.
- 476 Riechelmann, D.F.C., Deininger, M., Scholz, D., Riechelmann, S., Schröder-Ritzrau, A., Spötl, C.,
477 Richter, D.K., Mangini, A. and Immenhauser, A. (2013), Disequilibrium carbon and oxygen isotope
478 fractionation in recent cave calcite: Comparison of cave precipitates and model data, *Geochimica et*
479 *Cosmochimica Acta* 103, 232-244.
- 480 Scholz, D., C. Mühlinghaus, and A. Mangini (2009), Modelling $\delta^{13}\text{C}$ and $\delta^{18}\text{O}$ in the solution layer on
481 stalagmite surfaces, *Geochimica et Cosmochimica Acta*, 73(9), 2592-2602.
- 482 Spötl, C., I. J. Fairchild, and A. F. Tooth (2005), Cave air control on dripwater geochemistry, Obir
483 Caves (Austria): Implications for speleothem deposition in dynamically ventilated caves, *Geochimica*
484 *et Cosmochimica Acta*, 69(10), 2451-2468.
- 485 Stoll, H. M., A. Mendez-Vicente, S. Gonzalez-Lemos, A. Moreno, I. Cacho, H. Cheng, and R. L.
486 Edwards (2015), Interpretation of orbital scale variability in mid-latitude speleothem $\delta^{18}\text{O}$: Significance
487 of growth rate controlled kinetic fractionation effects, *Quaternary Science Reviews*.
- 488 Treble, P. C., J. Chappell, M. Gagan, K. McKeegan, and T. Harrison (2005), In situ measurement of
489 seasonal $\delta^{18}\text{O}$ variations and analysis of isotopic trends in a modern speleothem from southwest
490 Australia, *Earth and Planetary Science Letters*, 233(1-2), 17-32.
- 491 Treble, P. C., C. Bradley, A. Wood, A. Baker, C. N. Jex, I. J. Fairchild, M. K. Gagan, J. Cowley, and C.
492 Azcurra (2013), An isotopic and modelling study of flow paths and storage in Quaternary calcarenite,
493 SW Australia: implications for speleothem paleoclimate records, *Quaternary Science Reviews*, 64, 90-
494 103.
- 495 Treble, P. C., I. J. Fairchild, A. Griffiths, A. Baker, K. T. Meredith, A. Wood, and E. McGuire (2015),
496 Impacts of cave air ventilation and in-cave prior calcite precipitation on Golgotha Cave dripwater
497 chemistry, southwest Australia, *Quaternary Science Reviews*.
- 498 Treble, P. C., I. J. Fairchild, A. Baker, K. T. Meredith, M. S. Andersen, S. U. Salmon, C. Bradley, P. M.
499 Wynn, S. Hankin, A. Wood and E. McGuire (2016), Roles of forest bioproductivity, transpiration and
500 fire in a nine-year record of cave dripwater chemistry from southwest Australia, *Geochimica et*
501 *Cosmochimica Acta*, 184, 132-150.
- 502 Wong, C. I., and D. O. Breecker (2015), Advancements in the use of speleothems as climate archives,
503 *Quaternary Science Reviews*, 127, 1-18.
- 504
- 505
- 506